

# Weak Dirichlet Boundary Conditions for Wall-Bounded Turbulent Flows

Y. Bazilevs<sup>1</sup>, C. Michler<sup>1</sup>, V.M. Calo<sup>1</sup>, and T.J.R. Hughes<sup>2</sup>

*Institute for Computational Engineering and Sciences, The University of Texas at Austin,  
201 East 24th Street, 1 University Station C0200, Austin, TX 78712, USA*

---

## Abstract

In turbulence applications, strongly imposed no-slip conditions often lead to inaccurate mean flow quantities for coarse boundary-layer meshes. To circumvent this shortcoming, weakly imposed Dirichlet boundary conditions for fluid dynamics were recently introduced in [8]. In the present work, we propose a modification of the original weak boundary condition formulation that consistently incorporates the well-known “law of the wall”. To compare the different methods, we conduct numerical experiments for turbulent channel flow at Reynolds number 395 and 950. In the limit of vanishing mesh size in the wall-normal direction, the weak boundary condition acts like a strong boundary condition. Accordingly, strong and weak boundary conditions give essentially identical results on meshes that are stretched to better capture boundary layers. However, on uniform meshes that are incapable of resolving boundary layers, weakly imposed boundary conditions deliver significantly more accurate mean flow quantities than their strong counterparts. Hence, weakly imposed boundary conditions present a robust technique for flows of industrial interest, where optimal mesh design is usually not feasible and resolving boundary layers is prohibitively expensive. Our numerical results show that the formulation that incorporates the law of the wall yields an improvement over the original method.

*Key words:* fluids, Navier-Stokes equations, boundary layers, turbulence, law of the wall, weakly imposed boundary conditions, Isogeometric Analysis

---

<sup>1</sup> Postdoctoral Fellow

<sup>2</sup> Professor of Aerospace Engineering and Engineering Mechanics, Computational and Applied Mathematics Chair III

## 1 Introduction

In computational fluid dynamics formulations that employ continuous representation of the fields, Dirichlet boundary conditions are typically imposed by specifying the nodal values of the solution. This amounts to so-called “strong satisfaction” of the boundary conditions. In flow computations, strongly imposed no-slip conditions often lead to inaccurate mean flow quantities for insufficiently fine boundary-layer meshes. Recently, Bazilevs and Hughes [8] proposed to satisfy Dirichlet boundary conditions in a weak sense rather than strongly. To this end, the variational equations are augmented by terms that enforce the Dirichlet conditions weakly as Euler-Lagrange conditions. Thus, the functions representing the discrete solution are not required to satisfy the Dirichlet conditions explicitly. It was found that for the linear advection-diffusion equation it is precisely the weak Dirichlet boundary conditions that are able to mitigate or even entirely eliminate oscillations due to unresolved boundary layers as well as to improve the accuracy in the regions away from the layers. Moreover, numerical results for low Reynolds number flows computed on coarse meshes demonstrated that weak no-slip boundary conditions provide a significant increase in accuracy over their strong counterparts.

In the present work, we revisit the weak Dirichlet condition formulation. Although the design of the boundary condition is based on numerical rather than physical considerations, the weak treatment seems to behave like a wall function. To exploit this link with wall modeling, we propose a modification of the original formulation that consistently incorporates the well-known “law of the wall”, an empirical relation between the near-wall fluid velocity and the distance from the wall that is commonly assumed to hold for a broad range of Reynolds numbers [32]. We combine the weakly imposed boundary condition formulation with residual-based turbulence modeling, which is a new paradigm for computing turbulent flows introduced in [10, 21] and further developed in [4]. To compare the different Dirichlet boundary condition formulations, we assess their performance on turbulent channel flows at medium-to-high Reynolds numbers. These numerical test cases are more challenging than the ones considered previously in [8] due to the increased Reynolds number. In the limit of vanishing mesh size in the wall-normal direction, the weak formulation acts like a strong formulation. Accordingly, strong and weak formulations give essentially identical results on stretched meshes that are designed to better resolve the boundary layer. However, on meshes that are uniform also in the wall-normal direction, weakly imposed Dirichlet boundary conditions deliver significantly more accurate mean flow quantities than their strong counterparts. This fact makes the weakly enforced boundary condition formulations attractive for computing flows of industrial interest, allowing one to avoid the costly resolution of boundary layers without compromising the accuracy of large-scale features. We also find that the weak formulation modified to incorporate the law of the wall provides an improvement over the original formulation. Throughout this work, the spatial discretization makes use of the Isogeometric Analysis approach

[5, 7, 12, 22] that is based on NURBS (Non-uniform rational B-splines). Due to the rectangular geometry used for our numerical examples, NURBS reduce to standard B-splines.

The paper is organized as follows. In Section 2, we describe the weak formulation of the continuous problem for the incompressible Navier-Stokes equations. We then state the discrete, residual-based variational multiscale formulation of the problem with no-slip Dirichlet boundary conditions imposed weakly. In Section 3, we describe the new formulation with weakly imposed boundary conditions that incorporates the law of the wall by appropriately modifying the boundary terms of the original weak boundary condition formulation. In Section 4, we show numerical results for an equilibrium turbulent channel flow at Reynolds numbers 395 and 950 based on friction velocity. In all cases, we use meshes with orders of magnitude fewer grid points for our computations than the ones employed in high-fidelity Direct Numerical Simulation (DNS); see [13, 29]. In Section 5, we draw conclusions.

## 2 Weak Imposition of Dirichlet Boundary Conditions for Incompressible Navier-Stokes Equations

### 2.1 Continuous problem

We begin by considering a weak formulation of the Incompressible Navier-Stokes equations. Let  $\mathcal{V}$  denote the trial and weighting function spaces, which are assumed to be the same. We also assume  $\mathbf{u} = \mathbf{0}$  on  $\Gamma$  and  $\int_{\Omega} p(t) d\Omega = 0$  for all  $t \in ]0, T[$ . The variational formulation is stated as follows: Find a velocity-pressure pair,  $\mathbf{U} = \{\mathbf{u}, p\} \in \mathcal{V}$ , such that for all weighting functions  $\mathbf{W} = \{\mathbf{w}, q\} \in \mathcal{V}$

$$B(\mathbf{W}, \mathbf{U}) = (\mathbf{W}, \mathbf{F}), \quad (1)$$

where

$$B(\mathbf{W}, \mathbf{U}) = \left( \mathbf{w}, \frac{\partial \mathbf{u}}{\partial t} \right)_{\Omega} - (\nabla \mathbf{w}, \mathbf{u} \otimes \mathbf{u})_{\Omega} + (q, \nabla \cdot \mathbf{u})_{\Omega} - (\nabla \cdot \mathbf{w}, p)_{\Omega} + (\nabla^s \mathbf{w}, 2\nu \nabla^s \mathbf{u})_{\Omega}, \quad (2)$$

and

$$(\mathbf{W}, \mathbf{F}) = (\mathbf{w}, \mathbf{f})_{\Omega}. \quad (3)$$

In (2),  $\nu$  is the kinematic viscosity,  $p$  is the actual pressure divided by the fluid density, and  $\mathbf{f}$  is the body force.

Variational equations (1)-(3) imply satisfaction of the linear momentum equations

and of the incompressibility constraint, namely

$$\mathcal{L}(\mathbf{u}, p) - \mathbf{f} = \mathbf{0} \quad \text{in } \Omega, \quad (4)$$

$$\nabla \cdot \mathbf{u} = 0 \quad \text{in } \Omega, \quad (5)$$

where

$$\mathcal{L}(\mathbf{u}, p) = \frac{\partial \mathbf{u}}{\partial t} + \nabla \cdot (\mathbf{u} \otimes \mathbf{u}) + \nabla p - \nabla \cdot (2\nu \nabla^s \mathbf{u}). \quad (6)$$

We also introduce the ‘‘advective’’ form of the above operator

$$\mathcal{L}_{adv}(\mathbf{u}, p) = \frac{\partial \mathbf{u}}{\partial t} + \mathbf{u} \cdot \nabla \mathbf{u} + \nabla p - \nu \Delta \mathbf{u}, \quad (7)$$

which is obtained from (6) by using the incompressibility constraint in the advective term and in the viscous stress term.

## 2.2 Discrete formulation

Below, we recall the discrete variational formulation of the incompressible Navier-Stokes equations with weakly imposed Dirichlet boundary conditions; see also [8].

Let  $\Omega$  be decomposed into  $n_{el}$  elements, which induces the decomposition of  $\Gamma$  into  $n_{eb}$  boundary faces. We approximate (1)-(3) by the following variational problem over the finite-element spaces: Find  $\mathbf{U}^h = \{\mathbf{u}^h, p^h\} \in \mathcal{V}^h$ ,  $\mathbf{u}^h \cdot \mathbf{n} = 0$  on  $\Gamma$  such that  $\forall \mathbf{W}^h = \{\mathbf{w}^h, q^h\} \in \mathcal{V}^h$ ,  $\mathbf{w}^h \cdot \mathbf{n} = 0$  on  $\Gamma$ ,

$$\begin{aligned} B(\mathbf{W}^h, \mathbf{U}^h) - (\mathbf{w}^h, \mathbf{f})_\Omega & \quad (8) \\ & + \sum_{e=1}^{n_{el}} (\{\mathbf{u}^h \cdot \nabla \mathbf{w}^h + \nabla q^h\}_{\mathcal{T}_M}, \mathcal{L}_{adv}(\mathbf{u}^h, p^h) - \mathbf{f})_{\Omega_e} \\ & + \sum_{e=1}^{n_{el}} (\{\mathbf{u}^h \cdot (\nabla \mathbf{w}^h)^T\}_{\mathcal{T}_M}, \mathcal{L}_{adv}(\mathbf{u}^h, p^h) - \mathbf{f})_{\Omega_e} \\ & - \sum_{e=1}^{n_{el}} (\nabla \mathbf{w}^h, \tau_M \{\mathcal{L}_{adv}(\mathbf{u}^h, p^h) - \mathbf{f}\} \otimes \tau_M \{\mathcal{L}_{adv}(\mathbf{u}^h, p^h) - \mathbf{f}\})_{\Omega_e} \\ & + \sum_{e=1}^{n_{el}} (\nabla \cdot \mathbf{w}^h, \tau_C \nabla \cdot \mathbf{u}^h)_{\Omega_e} \\ & - \sum_{b=1}^{n_{eb}} (\mathbf{w}^h, 2\nu \nabla^s \mathbf{u}^h \cdot \mathbf{n})_{\Gamma_b \cap \Gamma} \\ & - \sum_{b=1}^{n_{eb}} (2\nu \nabla^s \mathbf{w}^h \cdot \mathbf{n}, \mathbf{u}^h - \mathbf{0})_{\Gamma_b \cap \Gamma} \\ & + \sum_{b=1}^{n_{eb}} (\mathbf{w}^h \frac{C_b^I \nu}{h_b}, \mathbf{u}^h - \mathbf{0})_{\Gamma_b \cap \Gamma} = 0, \end{aligned}$$

with the following definitions

$$\tau_M := \left( \frac{C_t}{\Delta t^2} + \mathbf{u}^h \cdot \mathbf{G} \mathbf{u}^h + C_I \nu^2 \mathbf{G} : \mathbf{G} \right)^{-1/2}, \quad (9)$$

and

$$\tau_C := (\mathbf{g} \cdot \tau_M \mathbf{g})^{-1}, \quad (10)$$

where  $\mathbf{G}$  is a second-rank metric tensor

$$\mathbf{G} = \left( \frac{\partial \boldsymbol{\xi}}{\partial \mathbf{x}} \right)^T \frac{\partial \boldsymbol{\xi}}{\partial \mathbf{x}}, \quad (11)$$

$\frac{\partial \boldsymbol{\xi}}{\partial \mathbf{x}}$  is the inverse Jacobian of the element mapping between the parent and the physical domain, and  $\mathbf{g}$  is a vector obtained by summing  $\frac{\partial \boldsymbol{\xi}}{\partial \mathbf{x}}$  on its first index as

$$\mathbf{g} = (\mathbf{g})_i = \sum_{j=1}^d \left( \frac{\partial \boldsymbol{\xi}}{\partial \mathbf{x}} \right)_{ji}. \quad (12)$$

Moreover, in (8)-(9),  $h_b$  is the wall-normal element mesh-size defined as

$$h_b = 2 \left( \mathbf{n}^T \mathbf{G} \mathbf{n} \right)^{-1/2}, \quad (13)$$

where  $\mathbf{n}$  is a unit outward normal vector to the fluid domain boundary, and  $C_I^b$ ,  $C_t$  and  $C_I$  are positive constants. Note that for rectangular meshes equation (13) gives the element length in the wall-normal direction.

## Remarks

- (1) The above formulation is a Residual-based Variational Multiscale Method for incompressible Navier-Stokes equations (see e.g. [4, 10, 21]) that is based on the variational multiscale methodology (VMS); see, e.g., [14, 17–20, 23]. In VMS, an a-priori decomposition of the trial and weighting function spaces into coarse and fine scales is employed. While the coarse scales are identified with the numerical approximation, the fine scales are associated with subgrid scales and thus need to be modeled. Here, a residual-based model is used for representing the fine scales. In particular, the fine scales are assumed to be proportional to the residuals of the large-scale equations with the proportionality factors  $\tau_M$  and  $\tau_C$ . Thus, the modeling is confined to the definition of the fine scales only.  $\tau_M$  is designed by asymptotic scaling (see [3]) developed within the theory of stabilized methods (see, e.g., [9, 16, 30, 33]). The definition of  $\tau_C$  derives from the fine-scale Schur complement operator for the pressure (see [4] for details). Thus, the residual-based methods possess a dual nature: on the one hand they are bona-fide LES-like turbulence models, and on the other hand they may be thought of as stabilized methods extended to the nonlinear realm.

- (2) The last three terms of (8) pertain to the weak enforcement of the no-slip condition, as presented in [8], inspired by the SIPG Discontinuous Galerkin method [34]. The third-to-last term in (8) is the so-called consistency term: When deriving the Euler-Lagrange equations corresponding to (8), integration-by-parts yields a term that is cancelled by the consistency term. The second-to-last term in (8) is the so-called adjoint-consistency term: If the exact solution of the adjoint problem is inserted into equation (8) in place of the test function, (8) is satisfied identically; see [2] for details on adjoint consistency. The last term of (8) penalizes the deviation of the discrete solution from the Dirichlet boundary condition.
- (3) We choose to enforce the normal component of the no-slip boundary condition, that is, the no-penetration condition, strongly on the trial and weighting function spaces.
- (4) In the case of strongly imposed no-slip conditions, the last three terms of (8) vanish.

### 3 Weakly Imposed No-Slip Dirichlet Boundary Conditions Based on a Wall Function Formulation

In this section, we revisit weakly imposed Dirichlet boundary conditions and propose a modification of the original formulation presented in the previous section. This modification draws on the knowledge of the fluid behavior in the vicinity of the wall in the regime of fully developed turbulence. In what follows, we reformulate the weakly imposed Dirichlet condition in a way that is consistent with the idea of wall modeling.

In engineering practice it is often of interest to accurately resolve large-scale flow features rather than fine-scale components. It is typically not the detailed features of the boundary-layer turbulence that are relevant for the application, but their effect on the overall flow behavior. This fact can be accounted for by wall modeling, in which the no-slip Dirichlet boundary condition is replaced by a traction Neumann boundary condition; see for example [28, p. 47]. A wall-shear-stress boundary condition is typically specified by adding the following term to the variational formulation

$$\sum_{b=1}^{n_{eb}} (\mathbf{w}^h, u^{*2} \frac{\mathbf{u}^h}{\|\mathbf{u}^h\|})_{\Gamma_b \cap \Gamma}, \quad (14)$$

where  $u^{*2}$  and  $\frac{\mathbf{u}^h}{\|\mathbf{u}^h\|}$  are the magnitude and the direction of the applied traction vector, respectively, and  $\|\cdot\|$  denotes the Euclidean length. The magnitude of the wall shear stress  $u^{*2}$  is consistent with the so-called “law of the wall”. This “law” is an empirical relation between the mean fluid speed and the normal distance to the wall. Among the many available parameterizations we employ the one given by

Spalding [32]

$$y^+ = f(u^+) = u^+ + e^{-\chi B} \left( e^{\chi u^+} - 1 - \chi u^+ - \frac{(\chi u^+)^2}{2} - \frac{(\chi u^+)^3}{6} \right), \quad (15a)$$

where  $y^+$  and  $u^+$  denote the distance from the wall and the mean fluid speed, respectively, expressed in non-dimensional wall units as

$$y^+ := \frac{y u^*}{\nu}, \quad (15b)$$

$$u^+ := \frac{\|\mathbf{u}^h\|}{u^*}. \quad (15c)$$

In equations (15b) and (15c),  $u^*$  is the friction velocity,  $y$  is the vertical distance to the wall,  $\mathbf{u}^h$  is the velocity parallel to the wall, and  $\chi = 0.4$  and  $B = 5.5$ . Spalding's parameterization of the turbulent boundary layer (15a) is valid over the entire range of  $y^+$ , from the viscous sublayer all the way to the end of the logarithmic layer.

Upon rearranging terms in (14), and dropping the sum over the element boundaries for brevity, the ‘‘penalty’’ structure of (14) becomes apparent, that is

$$\left( \mathbf{w}^h, u^{*2} \frac{\mathbf{u}^h}{\|\mathbf{u}^h\|} \right)_{\Gamma_b \cap \Gamma} = \left( \mathbf{w}^h \left[ \frac{u^{*2}}{\|\mathbf{u}^h\|} \right], \mathbf{u}^h - \mathbf{0} \right)_{\Gamma_b \cap \Gamma} = \left( \mathbf{w}^h \tau_B, \mathbf{u}^h - \mathbf{0} \right)_{\Gamma_b \cap \Gamma}, \quad (16)$$

with

$$\tau_B := \frac{u^{*2}}{\|\mathbf{u}^h\|} \quad (17)$$

acting as a penalty parameter. Based on this observation, we propose to modify the original weak boundary condition formulation (8) as follows: Find  $\mathbf{U}^h =$

$\{\mathbf{u}^h, p^h\} \in \mathcal{V}^h$ ,  $\mathbf{u}^h \cdot \mathbf{n} = 0$  on  $\Gamma$  such that  $\forall \mathbf{W}^h = \{\mathbf{w}^h, q^h\} \in \mathcal{V}^h$ ,  $\mathbf{w}^h \cdot \mathbf{n} = 0$  on  $\Gamma$ ,

$$\begin{aligned}
& B(\mathbf{W}^h, \mathbf{U}^h) - (\mathbf{w}^h, \mathbf{f})_\Omega \tag{18} \\
& + \sum_{e=1}^{n_{el}} (\{\mathbf{u}^h \cdot \nabla \mathbf{w}^h + \nabla q^h\}_{\mathcal{T}_M}, \mathcal{L}_{adv}(\mathbf{u}^h, p^h) - \mathbf{f})_{\Omega_e} \\
& + \sum_{e=1}^{n_{el}} (\{\mathbf{u}^h \cdot (\nabla \mathbf{w}^h)^T\}_{\mathcal{T}_M}, \mathcal{L}_{adv}(\mathbf{u}^h, p^h) - \mathbf{f})_{\Omega_e} \\
& - \sum_{e=1}^{n_{el}} (\nabla \mathbf{w}^h, \tau_M \{\mathcal{L}_{adv}(\mathbf{u}^h, p^h) - \mathbf{f}\} \otimes \tau_M \{\mathcal{L}_{adv}(\mathbf{u}^h, p^h) - \mathbf{f}\})_{\Omega_e} \\
& + \sum_{e=1}^{n_{el}} (\nabla \cdot \mathbf{w}^h, \tau_C \nabla \cdot \mathbf{u}^h)_{\Omega_e} \\
& - \sum_{b=1}^{n_{eb}} (\mathbf{w}^h, 2\nu \nabla^s \mathbf{u}^h \cdot \mathbf{n})_{\Gamma_b \cap \Gamma} \\
& - \sum_{b=1}^{n_{eb}} (2\nu \nabla^s \mathbf{w}^h \cdot \mathbf{n}, \mathbf{u}^h - \mathbf{0})_{\Gamma_b \cap \Gamma} \\
& \boxed{+ \sum_{b=1}^{n_{eb}} (\mathbf{w}^h \tau_B, \mathbf{u}^h - \mathbf{0})_{\Gamma_b \cap \Gamma}} = 0.
\end{aligned}$$

Variational equation (18) differs from (8) only in the last term on the left-hand side, and it may be thought of as a generalization of (8). Selecting  $y$  to be proportional to the wall-normal mesh size  $h_b$ , that is,  $y = h_b/C_b^I$ , and letting  $h_b$  go to zero, the Spalding equation (15a) reduces to  $y^+ = u^+$ , which is a well-known parameterization of the viscous sublayer. In this limit,  $\tau_B$  becomes independent of the slip velocity  $\mathbf{u}^h$  and takes on the expression

$$\tau_B = \frac{\nu}{y} = \frac{\nu C_b^I}{h_b}. \tag{19}$$

Thus, we recover the original weak formulation (8). This, in turn, implies that the formulation (18) inherits all the attributes of the original formulation (8) in this limit. Conversely, when the mesh size  $h_b$  is large,  $\tau_B$  deviates from (19).

Algorithm 1 outlines a Newton procedure to determine  $\tau_B$  from given  $\mathbf{u}^h$ ,  $h_b$  and  $\nu$  in accordance with the law-of-the-wall equation (15a). This procedure is local to each boundary-face integration point and, therefore, the cost associated with this algorithm is only a small fraction of the overall computational expense. Expression (19) with  $y = h_b/C_b^I$  is used to initialize  $\tau_B$ . In case  $\mathbf{u}^h$ ,  $h_b$  and  $\nu$  correspond to the viscous sublayer, the law-of-the-wall equation (15a) is satisfied by the initial

values, and no iteration is necessary. Algorithm 1 makes use of the Jacobian

$$\begin{aligned} \frac{\partial r}{\partial \tau_B} &= \frac{h_b}{2\nu C_b^I} \tau_{B,i}^{-1/2} \|\mathbf{u}^h\|^{1/2} \\ &+ \left( 1 + \chi e^{-\chi B} \left( e^{\chi u^+} - 1 - \chi u^+ - \frac{(\chi u^+)^2}{2} \right) \right) \frac{\tau_{B,i}^{-3/2}}{2} \|\mathbf{u}^h\|^{1/2}, \end{aligned} \quad (20)$$

where  $r := y^+ - f(u^+)$  is the residual of the Spalding equation (15a).

Alg. 1: Algorithm for computing  $\tau_B$ .

<ol style="list-style-type: none"> <li>1. Initialize iteration counter: <math>i = 0</math></li> <li>2. Initialize <math>\tau_{B,i} = C_b^I \frac{\nu}{h_b}</math></li> <li>3. <math>y_i^+ = u_i^+ = \tau_{B,i}^{-1/2} \ \mathbf{u}^h\ ^{1/2}</math></li> <li>4. <math>r_i = y_i^+ - f(u_i^+)</math></li> <li>5. <b>While</b> (<math> r_i  &gt; TOL</math>) <b>Do</b></li> <li>6.     <b>Build Jacobian:</b> <math>\frac{\partial r}{\partial \tau_B} _i</math> according to (20)</li> <li>7.     <b>Solve for increment:</b> <math>\Delta \tau_{B,i+1} = - \left( \frac{\partial r}{\partial \tau_B} _i \right)^{-1} r_i</math></li> <li>8.     <b>Update:</b> <math>\tau_{B,i+1} = \tau_{B,i} + \Delta \tau_{B,i+1}</math></li> <li>9.     <math>y_{i+1}^+ = \frac{h_b}{\nu C_b^I} \tau_{B,i+1}^{1/2} \ \mathbf{u}^h\ ^{1/2}</math></li> <li>10.     <math>u_{i+1}^+ = \tau_{B,i+1}^{-1/2} \ \mathbf{u}^h\ ^{1/2}</math></li> <li>11.     <math>r_{i+1} = y_{i+1}^+ - f(u_{i+1}^+)</math></li> <li>12.     <math>i = i + 1</math></li> <li>13. <b>Enddo</b></li> </ol>
---

## 4 Numerical experiments for turbulent channel flow

### 4.1 Problem setup

To investigate the performance of the weak boundary condition formulations, we conduct numerical experiments for turbulent channel flow at Reynolds numbers  $Re_\tau = 395$  and  $Re_\tau = 950$ , with  $Re_\tau$  based on the friction velocity and the channel half width. We compare the results with the formulation that imposes the no-slip condition strongly. To assess the accuracy of our methods, we compare our results to the DNS results of [29] for  $Re_\tau = 395$  and [13] for  $Re_\tau = 950$ .

The problem setup is shown in Figure 1. The flow is driven by a pressure gradient in the stream-wise direction. At the computational domain boundary, periodic boundary conditions are imposed in both stream-wise and span-wise directions, whereas a homogeneous Dirichlet boundary condition is applied in the wall-normal direction. Stream-wise and span-wise directions are commonly referred to as homogeneous directions.

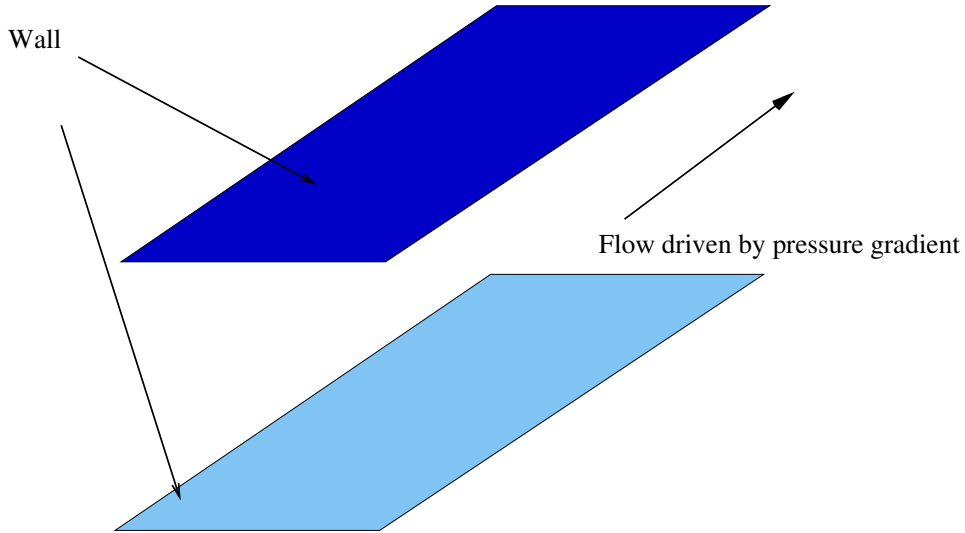


Fig. 1. Setup of turbulent channel flow problem.

For the spatial discretization we employ NURBS-based isogeometric analysis [22]. Our basis is comprised of quadratic B-spline functions that are  $C^1$ -continuous at knots. This is in contrast to standard quadratic finite-element functions that are only  $C^0$ -continuous across element boundaries. In recent studies we have found the NURBS discretization to be superior to standard finite elements on a per-degree-of-freedom basis for phenomena involving convection and diffusion, such as turbulent flow; see [1, 6, 12]. We also would like to point out that B-spline functions have been used for turbulence computations previously by [25–27, 31].

We employ meshes that are uniform in all directions and place the first knot in the wall-normal direction at the very beginning of the logarithmic layer. For comparison we also use meshes that are stretched in the wall-normal direction to cluster points near the boundary layer. The stretching is obtained by distributing the knots according to a hyperbolic tangent function such that the first knot lies at  $y^+ \approx 1.3$ , which is typical of Large Eddy Simulation (LES) computations. Details of the computational setup are shown in Table 1.

The semi-discrete equations are advanced in time using the generalized- $\alpha$  method with  $\rho_\infty = 0.5$ , where  $\rho_\infty$  is the spectral radius of the amplification matrix as  $\Delta t \rightarrow \infty$ , which controls high-frequency dissipation; see [11, 15, 24]. In all cases we use a time step of 0.025 based on the mean stream-wise flow velocity of unity. Moreover, we set  $C_t = 4$ ,  $C_I = 36$  and  $C_b^I = 4$ .

As initial condition we use a randomly perturbed Poiseuille flow profile. We perform time-integration until a statistically stationary, fully developed turbulent flow is reached. Further time-integration is carried out to collect statistics of the flow. Defining as a “flow-through” the time that it takes for a fluid particle to traverse the length of the channel, we collect data over ten flow-throughs, sampling twice per flow-through. Numerical results for all cases are reported in the form of statistics

of the mean velocity and root-mean-square of the velocity fluctuations. Statistics are computed by sampling the velocity field at the mesh knots and averaging the solution in time as well as in the stream-wise and span-wise directions. The mean velocity is typically referred to as the primary statistic, while the fluctuations are called secondary statistics. It is generally acknowledged that accuracy of the fluctuations is more difficult to achieve than accuracy of the mean velocity. Results are presented in non-dimensional wall units.

Table 1

Details of the computational setup.  $L_{x,y,z}$  denotes the length of the channel in the stream-wise, wall-normal and span-wise direction,  $N_{el}$  is the number of elements in the domain,  $N_{x,y,z}$  is the number of basis functions in the stream-wise, wall-normal and span-wise direction,  $f_x$  is the forcing in the stream-wise direction, and  $\nu$  denotes kinematic viscosity.

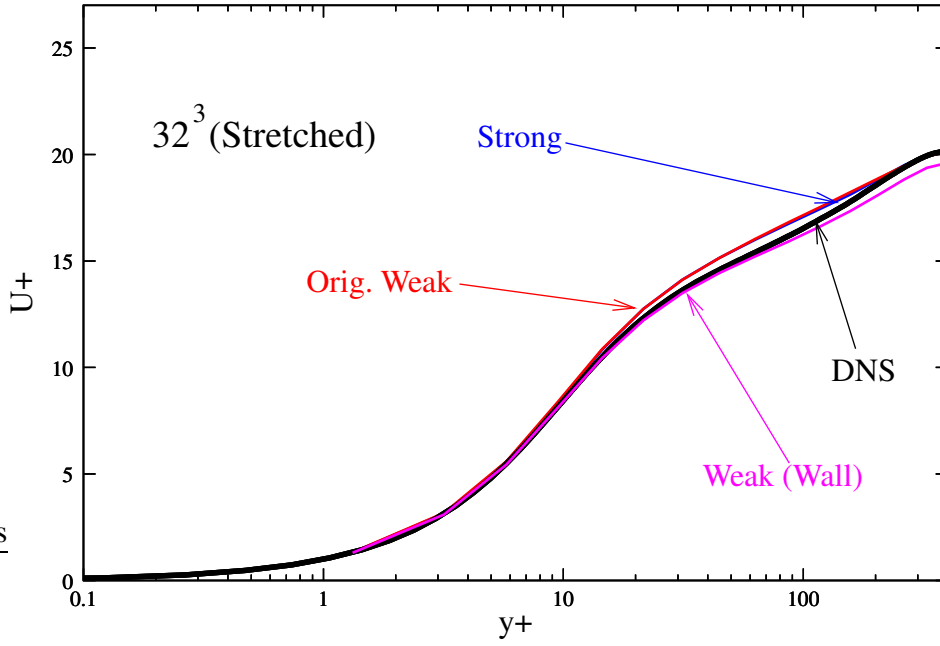
	$L_x$	$L_y$	$L_z$	$N_{el}$	$N_x$	$N_y$	$N_z$	$f_x$	$\nu$
$Re = 395$	$2\pi$	2	$\frac{2}{3}\pi$	$32^3$	32	34	32	$3.372040 \cdot 10^{-3}$	$1.47200 \cdot 10^{-4}$
$Re = 950$	$4\pi$	2	$\frac{4}{3}\pi$	$64^3$	64	66	64	$2.630991 \cdot 10^{-3}$	$0.53992 \cdot 10^{-4}$

#### 4.2 Turbulent channel flow at $Re_\tau = 395$

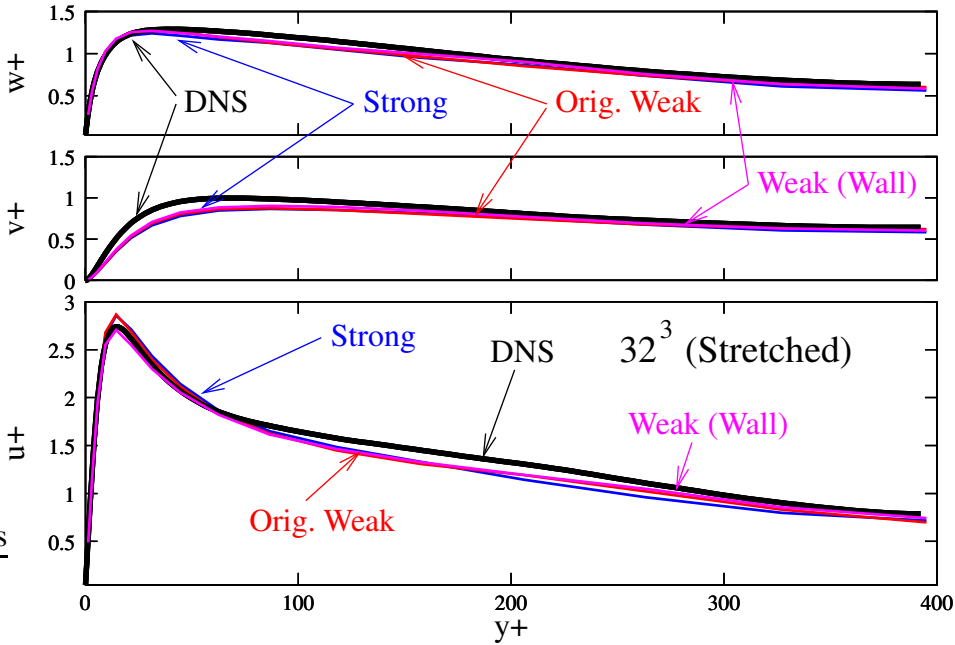
Our computations are carried out on a mesh of  $32^3$  elements. This discretization gives 32 basis functions in the homogeneous directions and 34 basis functions in the wall-normal direction due to the open knot vector construction (see [22] for details). In terms of the number of degrees-of-freedom, this type of resolution is typical of LES at Reynolds number 395. The domain size is  $2\pi$ , 2, and  $2/3\pi$  in the stream-wise, wall-normal, and span-wise directions, respectively. The corresponding DNS computation was carried out on a domain of the size  $2\pi \times 2 \times \pi$ , and the discretization used  $256 \times 193 \times 192$  spectral functions in the stream-wise, wall-normal and span-wise direction, respectively.

Figures 2 and 3 show statistics of the computations on the stretched and uniform meshes, respectively.

On the stretched mesh, both the mean flow and the fluctuations are in very good agreement with the DNS (see Figure 2). In fact, the quality of the results is virtually that of an accurate spectral LES computation (see [19]), although simple quadratic spline functions with local support are used instead of spectral basis functions. Results obtained with strongly and weakly imposed no-slip conditions practically coincide, which is consistent with the fact that the weak boundary condition formulation reduces to the strong one in the limit of vanishing mesh size. The newly



(a) Mean stream-wise velocity

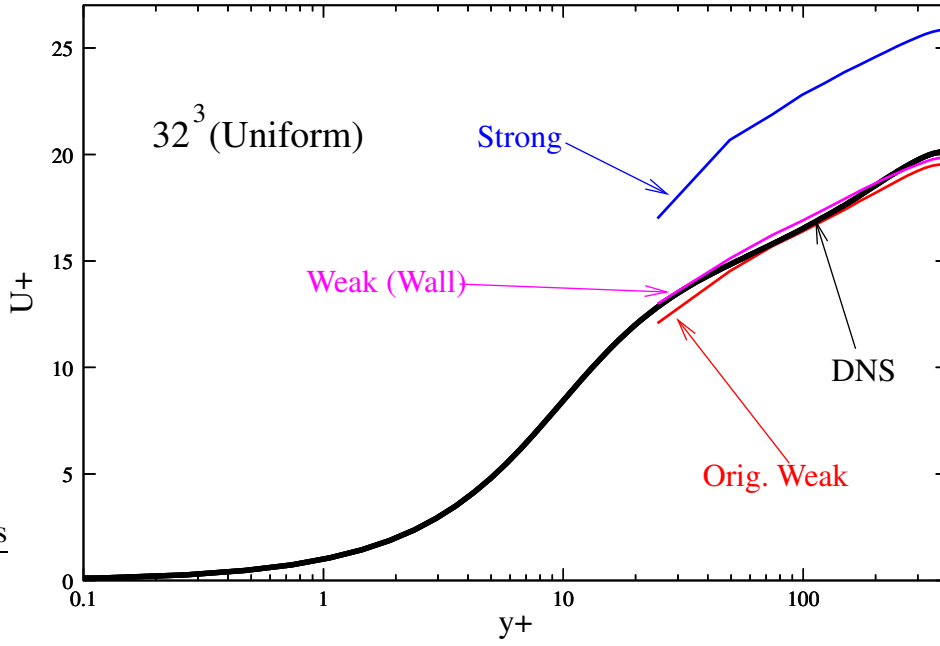


(b) Velocity fluctuations

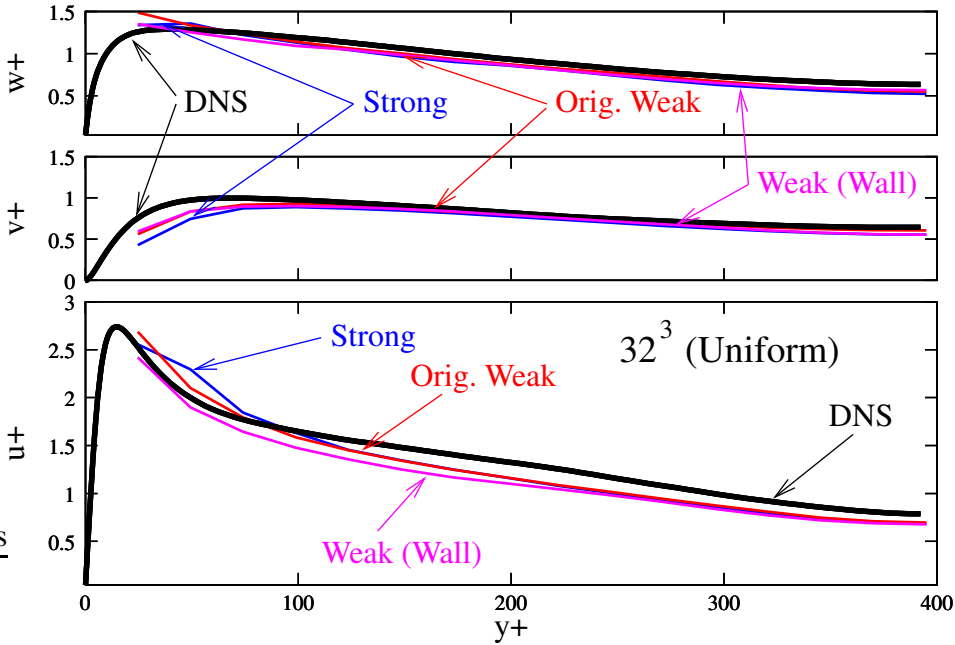
Fig. 2. Turbulent channel flow at  $Re_\tau = 395$  computed on a *stretched* mesh. Formulation with no-slip boundary conditions enforced strongly (**Strong**), weakly according to original methodology (8) (**Orig. Weak**), and weakly based on the wall function (18) (**Weak (Wall)**).

proposed formulation that incorporates wall modeling gives slightly more accurate stream-wise velocity fluctuations than the other formulations.

In contrast, on the uniform mesh, the methods perform differently (see Figure 3).



(a) Mean stream-wise velocity



(b) Velocity fluctuations

Fig. 3. Turbulent channel flow at  $Re_\tau = 395$  computed on a *uniform* mesh. Formulation with no-slip boundary conditions enforced strongly (**Strong**), weakly according to original methodology (8) (**Orig. Weak**), and weakly based on the wall function (18) (**Weak(Wall)**).

Using 32 equispaced elements in the wall normal direction places the first knot at  $y^+ \approx 23$ . Thus, we intentionally sacrifice the resolution of the boundary layer. This leads to a gross overestimation of the mean flow for the strongly enforced Dirichlet boundary condition formulation. Note that, on the other hand, the mean velocity

for both weak formulations agrees very well with the DNS result. This shows that weak boundary conditions are capable of alleviating the gross inaccuracy induced by insufficient near-wall resolution. This superior robustness despite “poor” mesh design makes the new method attractive for industrial applications. We also note that the wall function formulation is slightly more accurate for mean flow velocity than the original weak boundary condition formulation. Despite the large difference in the mean flow, the secondary statistics in the core of the channel for the uniform mesh cases are very similar for all formulations considered. In the near wall region, the differences in the fluctuations obtained with the various methods are more pronounced.

Comparing the results obtained on stretched and on uniform meshes, we observe that the secondary statistics for the uniform mesh simulations are not quite as accurate as those for the stretched grid case, although the quality of the results is still good. One may thus conclude that in the core of the channel the effect of the mesh design on the fluctuations is more pronounced than the effect of the boundary conditions.

Figure 4 shows the stream-wise velocity contours at an instant in time, computed on a uniform mesh with weak boundary conditions employing the wall function formulation. Note the presence of velocity fluctuations of considerable magnitude at the “no-slip” wall (see top surface of the box).

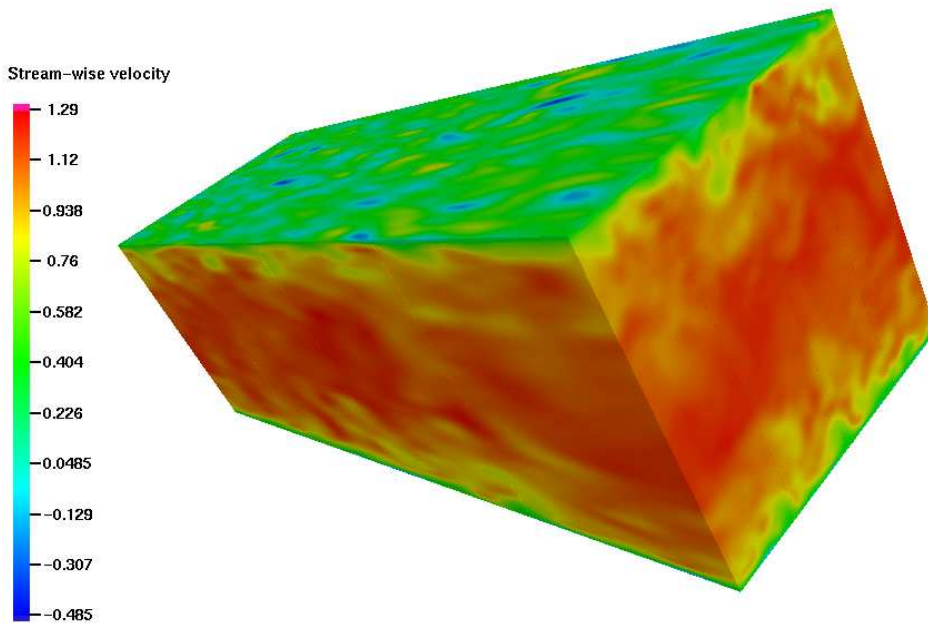


Fig. 4. Turbulent channel flow at  $Re_\tau = 395$ . Snapshot of stream-wise velocity contours.

### 4.3 Turbulent channel flow at $Re_\tau = 950$

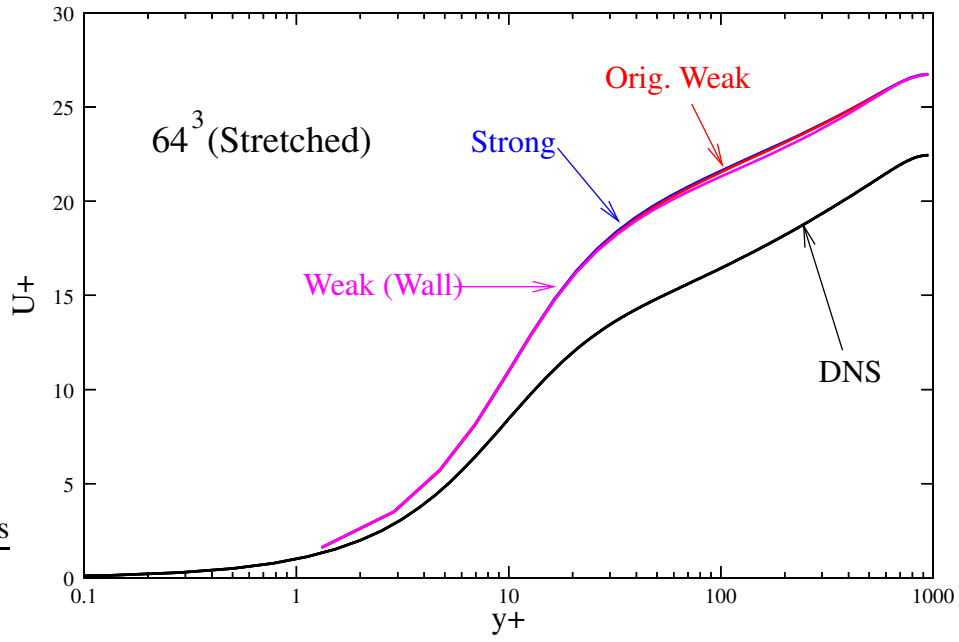
For the computations at  $Re_\tau = 950$ , a mesh of  $64^3$  elements is used with 64 basis functions in the homogeneous directions and 66 basis function in the wall-normal direction due to the open knot vector construction. The domain size is  $4\pi$ , 2, and  $4/3\pi$  in the stream-wise, wall-normal and span-wise directions, respectively. The corresponding DNS used a domain size of  $8\pi \times 2 \times 3\pi$  with a resolution of  $3072 \times 385 \times 2304$  spectral functions in the stream-wise, wall-normal and span-wise directions. Note that our resolution per unit domain length is a factor of about 24 coarser in the stream-wise direction, a factor of 6 coarser in the wall-normal direction, and a factor of 16 coarser in the span-wise direction. Hence, the adopted discretization is significantly coarser than what is typically used for an LES-type computation.

Figures 5 and 6 show statistics of the computations on stretched and uniform meshes, respectively.

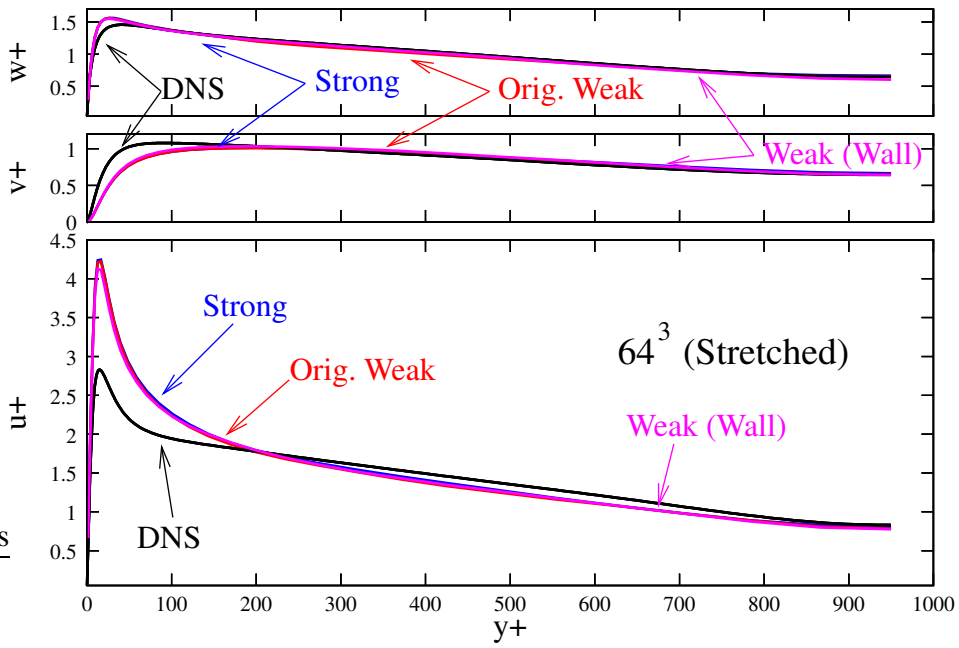
On a stretched mesh, the differences between the weak and the strong boundary-condition formulations are negligible due to the small near-wall mesh size in the wall-normal direction (see Figure 5). All methods fail to accurately represent the mean flow velocity. Moreover, the stream-wise velocity fluctuations are inaccurate in the near-wall region but are quite accurate in the core of the channel. The velocity fluctuations in the remaining directions are in very good agreement with the DNS. The good agreement of the velocity fluctuations with the DNS despite the discrepancy in the mean flow velocity is somewhat surprising. The inability to accurately capture the mean velocity illustrates the limitations of the strong boundary-condition method for high Reynolds number wall-bounded flows.

On the uniform mesh, with the first knot at  $y^+ \approx 30$ , the strong boundary condition formulation gives an even greater over-prediction of the mean velocity than for the stretched mesh computations; compare Figures 5 and 6. In contrast, both weak boundary-condition formulations deliver a result of reasonable accuracy for such a coarse discretization, similar to the case of  $Re_\tau = 395$ . The mean flow is only slightly over-predicted when compared to the DNS. Also note that the uniform discretization does not exhibit as severe an overshoot in the stream-wise velocity fluctuations near the wall as for the stretched mesh. However, away from the wall, the fluctuations are slightly less accurate on the uniform mesh than on the stretched mesh. This is consistent with the results for the  $Re_\tau = 395$  case.

Figure 7 shows the stream-wise velocity contours at an instant in time, computed on a uniform mesh with weak boundary conditions employing the wall function formulation. Note the presence of velocity fluctuations of considerable magnitude at the “no-slip” wall (see top surface of the box). Also note that the turbulent structures for the  $Re_\tau = 950$  channel are more fine-grained than the ones for the  $Re_\tau = 395$



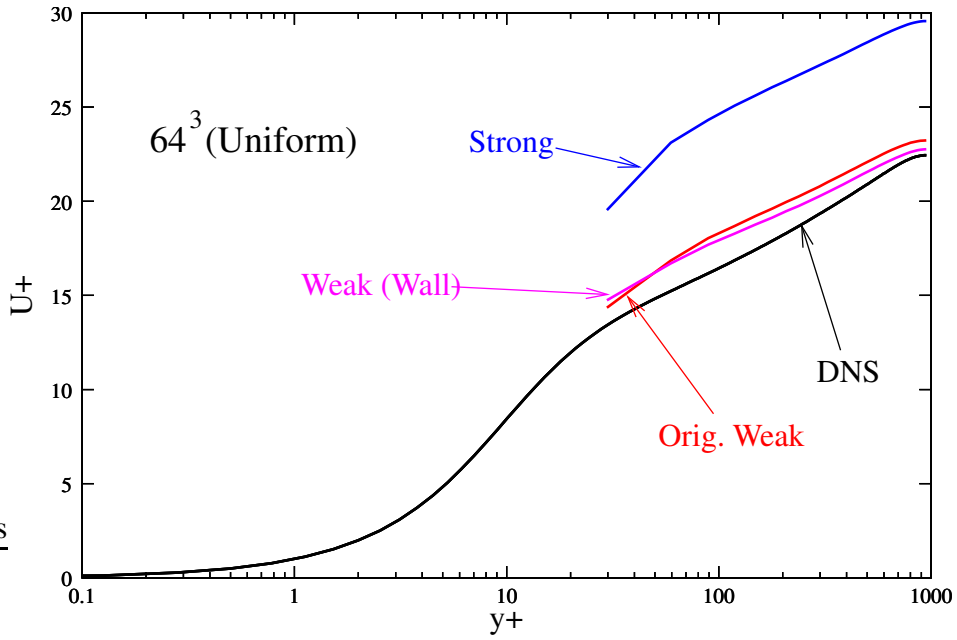
(a) Mean stream-wise velocity



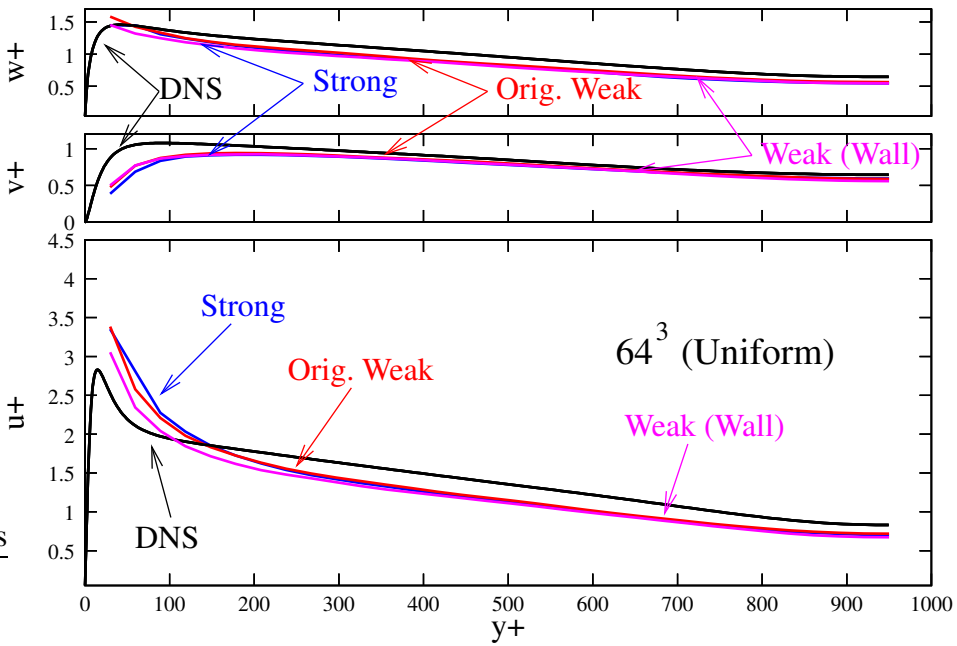
(b) Velocity fluctuations

Fig. 5. Turbulent channel flow at  $Re_\tau = 950$  computed on a *stretched* mesh. Formulation with no-slip boundary conditions enforced strongly (**Strong**), weakly according to original methodology (8) (**Orig. Weak**), and weakly based on the wall function (18) (**Weak (Wall)**).

channel due to the increased Reynolds number (compare Figures 4 and 7).



(a) Mean stream-wise velocity



(b) Velocity fluctuations

Fig. 6. Turbulent channel flow at  $Re_\tau = 950$  computed on a *uniform* mesh. Formulation with no-slip boundary conditions enforced strongly (**Strong**), weakly according to original methodology (8) (**Orig. Weak**), and weakly based on the wall function (18) (**Weak (Wall)**).

## 5 Conclusions

In this work, we proposed a new variational formulation of the incompressible Navier-Stokes equations that enforces Dirichlet no-slip boundary conditions weakly.

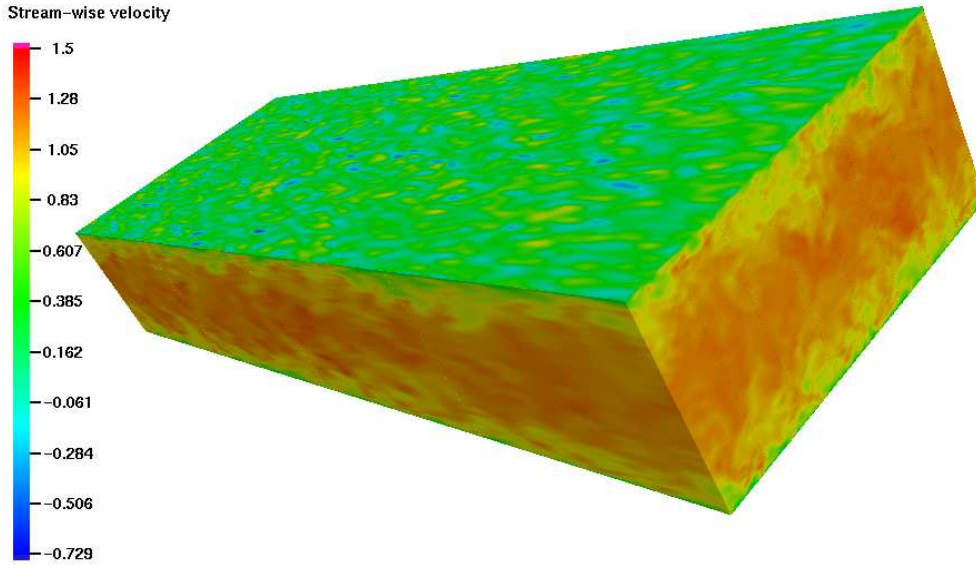


Fig. 7. Turbulent channel flow at  $Re_\tau = 950$ . Snapshot of stream-wise velocity contours.

Motivated by the observation that weak imposition of Dirichlet boundary conditions generally seems to behave like a wall function, the proposed formulation is based on the so-called law of the wall. We combined the weak boundary condition formulation with residual-based turbulence modeling. We compared the performance of the different boundary condition formulations based on numerical results for turbulent channel flow at medium-to-high Reynolds number. We found that the weakly imposed boundary condition formulation that incorporates the law of the wall provides an improvement over the original weak boundary condition formulation. In the limit of vanishing mesh size in the wall-normal direction, both weak boundary condition formulations act like a strong formulation. Accordingly, weak and strong boundary condition formulations give essentially identical results on stretched meshes that are designed to better capture the boundary layer. However, on coarse, uniform meshes, weakly imposed boundary conditions deliver a significantly more accurate mean flow velocity than their strong counterpart. In this respect, the combination of residual-based turbulence modeling and weak imposition of the no-slip condition acts like a RANS-type model in the sense that it produces accurate mean flow quantities on meshes that are too coarse for conventional LES simulations. This result makes weakly imposed Dirichlet boundary condition formulations attractive for computing flows of industrial interest, avoiding the costly resolution of boundary layers without compromising the accuracy of large-scale flow features. Given that the weak boundary condition formulation behaves like its strong counterpart on fine meshes and delivers superior accuracy on coarse meshes, this suggests the use of this method as a general strategy for enforcing wall boundary conditions in finite-element flow computations. The additional cost due to weak enforcement of the boundary conditions is negligible because the

corresponding integrals are evaluated only over the Dirichlet portion of the domain boundary.

Regarding the role of weak versus strong boundary condition formulation in the context of residual-based turbulence modeling, our results for the  $Re_\tau = 395$  channel flow show that the residual-based formulation with standard strongly imposed boundary conditions gives remarkably accurate results for a well designed, stretched mesh with a resolution that is typical of LES. However, for flows at higher Reynolds number, such as  $Re_\tau = 950$  computed on a stretched mesh with a resolution corresponding to coarse LES / fine RANS, the accuracy of the stand-alone residual-based approach deteriorates. The lack of accuracy in predicting the mean flow velocity derives from the inability to resolve the turbulent-boundary-layer flow structures on a mesh that is insufficiently fine. Our results demonstrate that this difficulty can be elegantly circumvented by combining the residual-based formulation with a weakly enforced no-slip boundary condition.

## Acknowledgments

This research was supported by Office of Naval Research Contract N00014-03-0263, Dr. Luise Couchman, contract monitor, and Sandia National Laboratories under contract number 114166. Y. Bazilevs and C. Michler were partially supported by the J.T. Oden ICES Postdoctoral Fellowship at the Institute for Computational Engineering and Sciences (ICES), and C. Michler was also supported through a stipend from the Netherlands Organization for Scientific Research (NWO). This support is gratefully acknowledged. The authors would also like to thank Nathan Brasher for his assistance with flow visualization.

## References

- [1] I. Akkerman, Y. Bazilevs, V. M. Calo, T. J. R. Hughes, and S. Hulshoff. The role of continuity in residual-based variational multiscale modeling of turbulence. 2007. Preprint.
- [2] D.N. Arnold, F. Brezzi, B. Cockburn, and L.D. Marini. Unified analysis of Discontinuous Galerkin methods for elliptic problems. *SIAM Journal of Numerical Analysis*, 39:1749–1779, 2002.
- [3] G. I. Barenblatt. *Similarity, self-similarity, and intermediate asymptotics*. Consultants Bureau, Plenum Press, New York and London, 1979.
- [4] Y. Bazilevs. *Isogeometric Analysis of Turbulence and Fluid-Structure Interaction*. PhD thesis, ICES, UT Austin, 2006.
- [5] Y. Bazilevs, V. M. Calo, Y. Zhang, and T. J. R. Hughes. Isogeometric fluid-

- structure interaction analysis with applications to arterial blood flow. *Computational Mechanics*, 38:310–322, 2006.
- [6] Y. Bazilevs, V.M. Calo, J.A. Cottrell, T.J.R. Hughes, A. Reali, and G. Scovazzi. Variational multiscale residual-based turbulence modeling for large eddy simulation of incompressible flows. 2007. Preprint.
- [7] Y. Bazilevs, L. Beirao da Veiga, J.A. Cottrell, T.J.R. Hughes, and G. Sangalli. Isogeometric analysis: Approximation, stability and error estimates for  $h$ -refined meshes. *Mathematical Models and Methods in Applied Sciences*, 16:1031–1090, 2006.
- [8] Y. Bazilevs and T.J.R. Hughes. Weak imposition of Dirichlet boundary conditions in fluid mechanics. *Computers and Fluids*, 36:12–26, 2007.
- [9] A. N. Brooks and T. J. R. Hughes. Streamline upwind / Petrov-Galerkin formulations for convection dominated flows with particular emphasis on the incompressible Navier-Stokes equations. *Computer Methods in Applied Mechanics and Engineering*, 32:199–259, 1982.
- [10] V.M. Calo. *Residual-based Multiscale Turbulence Modeling: Finite Volume Simulation of Bypass Transition*. PhD thesis, Department of Civil and Environmental Engineering, Stanford University, 2004.
- [11] J. Chung and G. M. Hulbert. A time integration algorithm for structural dynamics with improved numerical dissipation: The generalized- $\alpha$  method. *Journal of Applied Mechanics*, 60:371–75, 1993.
- [12] J.A. Cottrell, A. Reali, Y. Bazilevs, and T.J.R. Hughes. Isogeometric analysis of structural vibrations. *Computer Methods in Applied Mechanics and Engineering*, 195:5257–5297, 2006.
- [13] J. C. del Alamo, J. Jimenez, P. Zandonade, and R. D. Moser. Scaling of the energy spectra of turbulent channels. *Journal of Fluid Mechanics*, 500:135–144, 2004.
- [14] J. Holmen, T.J.R. Hughes, A.A. Oberai, and G.N. Wells. Sensitivity of the scale partition for variational multiscale LES of channel flow. *Physics of Fluids*, 16(3):824–827, 2004.
- [15] T. J. R. Hughes. *The Finite Element Method: Linear Static and Dynamic Finite Element Analysis*. Dover Publications, Mineola, NY, 2000.
- [16] T. J. R. Hughes and M. Mallet. A new finite element formulation for fluid dynamics: III. The generalized streamline operator for multidimensional advective-diffusive systems. *Computer Methods in Applied Mechanics and Engineering*, 58:305–328, 1986.
- [17] T. J. R. Hughes, L. Mazzei, and K. E. Jansen. Large-eddy simulation and the variational multiscale method. *Computing and Visualization in Science*, 3:47–59, 2000.
- [18] T. J. R. Hughes, L. Mazzei, A. A. Oberai, and A.A. Wray. The multiscale formulation of large eddy simulation: Decay of homogenous isotropic turbulence. *Physics of Fluids*, 13(2):505–512, 2001.
- [19] T. J. R. Hughes, A. A. Oberai, and L. Mazzei. Large-eddy simulation of turbulent channel flows by the variational multiscale method. *Physics of Fluids*, 13(6):1784–1799, 2001.

- [20] T. J. R. Hughes, G. Scovazzi, and L. P. Franca. Multiscale and stabilized methods. In E. Stein, R. de Borst, and T. J. R. Hughes, editors, *Encyclopedia of Computational Mechanics, Vol. 3, Computational Fluid Dynamics*, chapter 2. Wiley, 2004.
- [21] T.J.R. Hughes, V.M. Calo, and G. Scovazzi. Variational and multiscale methods in turbulence. In W. Gutkowsky and T.A. Kowalewski, editors, *In Proceedings of the XXI International Congress of Theoretical and Applied Mechanics (IUTAM)*. Kluwer, 2004.
- [22] T.J.R. Hughes, J.A. Cottrell, and Y. Bazilevs. Isogeometric analysis: CAD, finite elements, NURBS, exact geometry, and mesh refinement. *Computer Methods in Applied Mechanics and Engineering*, 194:4135–4195, 2005.
- [23] T.J.R. Hughes, G.N. Wells, and A.A. Wray. Energy transfers and spectral eddy viscosity of homogeneous isotropic turbulence: comparison of dynamic Smagorinsky and multiscale models over a range of discretizations. *Physics of Fluids*, 16:4044–4052, 2004.
- [24] K. E. Jansen, C. H. Whiting, and G. M. Hulbert. A generalized- $\alpha$  method for integrating the filtered Navier-Stokes equations with a stabilized finite element method. *Computer Methods in Applied Mechanics and Engineering*, 190:305–319, 1999.
- [25] A. G. Kravchenko, P. Moin, and R. Moser. Zonal embedded grids for numerical simulation of wall-bounded turbulent flows. *Journal of Computational Physics*, 127:412–423, 1996.
- [26] A. G. Kravchenko, P. Moin, and K. Shariff. B-spline method and zonal grids for simulation of complex turbulent flows. *Journal of Computational Physics*, 151:757–789, 1999.
- [27] W. Y. Kwok, R. D. Moser, and J. Jiménez. A critical evaluation of the resolution properties of B-spline and compact finite difference methods. *Journal of Computational Physics*, 174:510–551, 2001.
- [28] B. Mohammadi and O. Pironneau. *Analysis of the K-Epsilon turbulence model*. John Wiley & Sons, Chichester, England, 1994.
- [29] R. Moser, J. Kim, and R. Mansour. DNS of turbulent channel flow up to  $Re=590$ . *Physics of Fluids*, 11:943–945, 1999.
- [30] F. Shakib, T. J. R. Hughes, and Z. Johan. A new finite element formulation for computational fluid dynamics: X. The compressible Euler and Navier-Stokes equations. *Computer Methods in Applied Mechanics and Engineering*, 89:141–219, 1991.
- [31] K. Shariff and R. D. Moser. Two-dimensional mesh embedding for B-spline methods. *Journal of Computational Physics*, 145:471–488, 1998.
- [32] D.B. Spalding. A single formula for the law of the wall. *Journal of Applied Mechanics*, 28:444–458, 1961.
- [33] T.E. Tezduyar. Computation of moving boundaries and interfaces and stabilization parameters. *International Journal of Numerical Methods in Fluids*, 43:555–575, 2003.
- [34] M.F. Wheeler. An elliptic collocation-finite element method with interior penalties. *SIAM Journal of Numerical Analysis*, 15:152–161, 1978.